Acta Geophysica (2022) 70:1241–1252
https://doi.org/10.1007/s11600-022-00770-2

RESEARCH ARTICLE - ANTHROPOGENIC GEOHAZARDS

The aftershock sequence at a deep nickel mine: temporal and spatial distribution, magnitude distribution, and aftershock decay following major events

Xu Ma[1,2] · Erik Westman[2] · Farid Malek[3] · Baisheng Nie[4,5] · Shuangshuang Lin[5]

Received: 20 February 2021 / Accepted: 16 March 2022 / Published online: 8 April 2022

Abstract

Mining-induced seismic events greatly threaten safety of underground workers and studying major seismic events would help mitigate hazards in deep mines. Characterizing the aftershock sequence of major events can contribute to developing a reentry protocol after major events occur at mines. This study uses two major events and their aftershock sequences at Creighton Mine to investigate properties of aftershock sequences focusing on the magnitude of completeness and aftershock decay pattern. Two major events with moment magnitude 3.1 and 1.4 are analyzed, respectively, and their aftershock sequence are examined in this study. The optimal magnitude of completeness is rigorously determined by evaluating the goodness of fit using the maximum likelihood method. Then, parameters of aftershock decay using the MOL are estimated. We identify that the *p*-value of the two studied events is slightly larger than 0.8. This parametrization process using the MOL can assist in better understanding aftershock sequences of mining-induced major events and therefore mitigating seismic hazards in mining by potentially helping establish a reentry protocol based on the seismicity dropping below a certain rate. For establishing a reentry protocol, the study of the two events can be considered as a methodological work and a future statistical work for many events with different magnitudes and locations to establish the range of the MOL parameters is needed.

Keywords Mining-induced seismicity · Rock bursts · Aftershock decay · The MOL

Edited by Prof. Savka Dineva (CO-EDITOR-IN-CHIEF).

✉ Xu Ma
xuma@vt.edu

1 State Key Laboratory of Earthquake Dynamics, Institute of Geology, China Earthquake Administration, Beijing, China

2 Department of Mining and Minerals Engineering, Virginia Tech, Blacksburg, VA 24060, USA

3 Creighton Mine, Vale Canada Limited, Sudbury, ON, Canada

4 School of Resources and Safety Engineering, Chongqing University, Chongqing, China

5 School of Emergency Management and Safety Engineering, China University of Mining and Technology (Beijing), Beijing, China

Graphical abstract

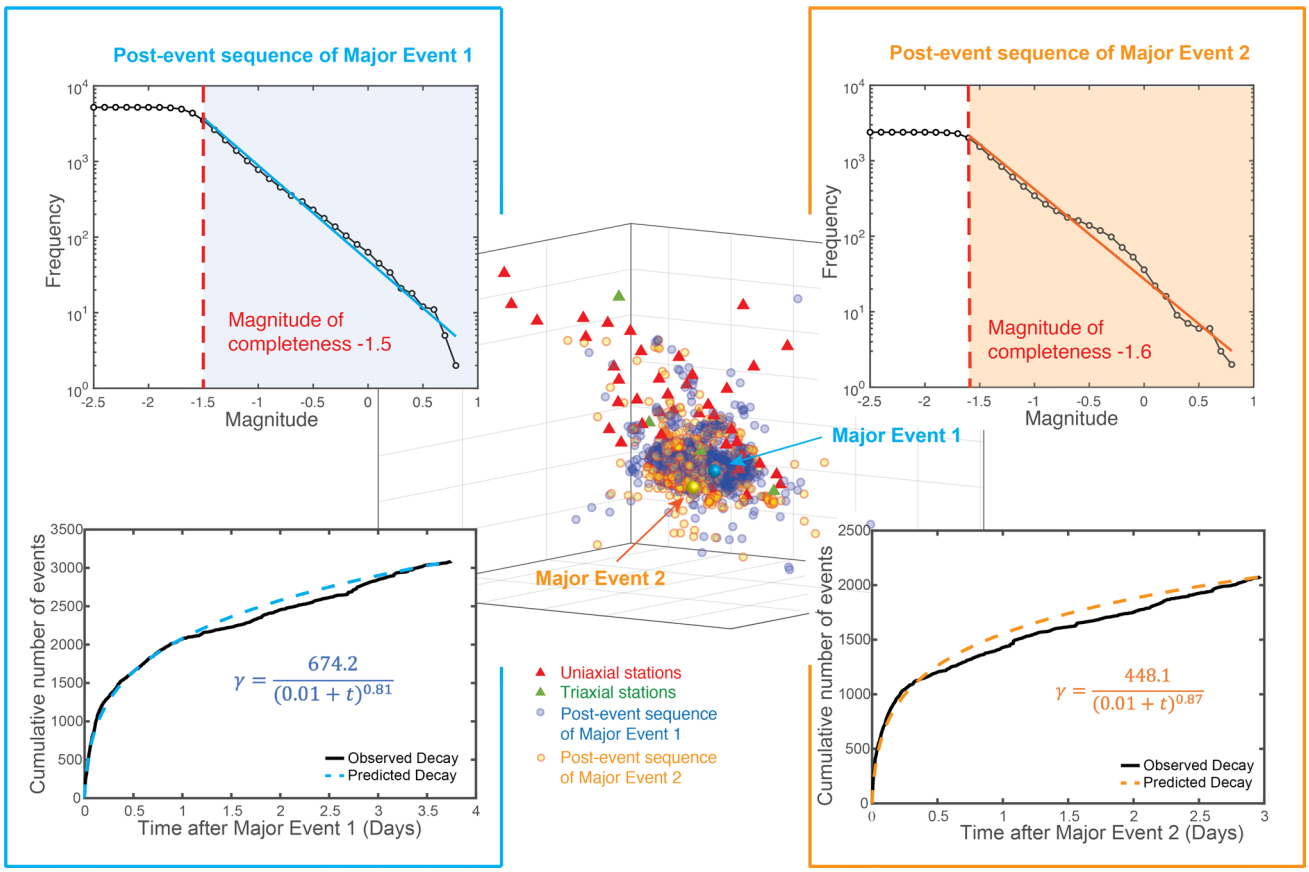

Introduction

Mining operations are conducted at great depths and will continue even deeper excavations in the long term to meet the increasing demand of mineral resources. Stress perturbations caused by mining operations, associated with great depths and geological structures such as faults and joints, inevitably lead to the mining-induced seismic events with high magnitude that are harmful for mining safety (Young and Maxwell 1992; Urbancic et al. 1993; Goebel et al. 2013; Ma et al. 2016; Xu and Cai 2017). To mitigate seismic hazards in mining, seismic monitoring technology has been widely used in mines in the last decade (Luxbacher et al. 2008; Hudyma and Potvin 2010; Brown and Hudyma 2017a). Microseismic monitoring has been making a difference in the mining industry by helping mining-industry workers prepare and keep them alerted about mining-induced seismicity and the threats the seismicity poses (Brady and Brown 2007; Brady and Leighton 1977; Beck and Brady 2002). The number of incidents from major events (rock bursts) can be limited and prevented so that losses from casualty and damaged equipment would be lessened (Bogucki et al. 2016).

Previous studies applied techniques and theories from seismology, such as seismic imaging, moment tensor, and *b*-value examination, in mining-induced seismicity and have resulted in a better understanding of mining-induced seismicity (Luxbacher et al. 2008; Barton and Pandey 2011; Ma et al. 2016; Brown and Hudyma 2017b). With this knowledge, early warning systems have been developed for alerting major events. In crustal earthquake studies, magnitude distribution based on the Gutenberg–Richter law and the MOL was further developed for characterizing aftershock using a stochastic model (Utsu 1961; Kisslinger and Jones 1991; Utsu et al. 1995). The MOL model has been widely used in crustal earthquakes and induced seismicity of oil gas fields to estimate the decay pattern of seismicity rate, post seismic events productivity, and other temporal-spatial interplays between seismic events (Llenos and Michael 2013). Using the Gutenberg–Richter law and the MOL, some studies developed reentry protocols and the guidelines for reentry protocols applicable to the mines located in Ontario,

Canada were justified (Vallejos and McKinnon 2009; Vallejos and McKinnon 2011; Tierney and Morkel 2017; Vallejos and Estay 2018). The successful reentry protocols can minimize the period of exclusion from entering mining regions while maximizing the inclusion of high magnitude events within the exclusion period (Tierney and Morkel 2017). Vallejos and McKinnon (2011) suggested a method of using an approximately constant level to quantify the background levels of seismicity rate. The method of establishing a reentry protocol on the basis of source parameters, including static/dynamic stress drop and apparent stress variation, was also proposed (Disley 2014).

Aftershock in order to improve the knowledge of mining-induced seismic events, seismic monitoring systems have been widely used in underground mining. The quantification and characterization of seismic events can assist in understanding the mechanism of inducing seismic events and mitigating seismic hazards in underground mines. Aftershock decay plays an important role in examining and estimating the potential of seismic hazards threating mining safety (Omi et al. 2013). The background for this study is that the aftershock decay following the occurrence of major events is crucial for developing a reentry protocol for mines. The MOL model is applied in this work to examine aftershock decay and rock mass behavior related to two major events. The application of aftershock decay in mining-induced seismicity can illuminate the aftershock decay following major events. This research aims to investigate aftershock decay at a hard-rock underground mine, thereby mitigating seismic hazards and improving safety of deep hard-rock underground mines by setting up reentry protocol. Because mines have worked to establish a reentry protocol based on seismicity dropping below a certain rate of seismic events, this study could be used to help establish the reentry protocol, and to specifically provide an earlier estimate of the safety criteria to reenter underground in terms of elapsed time after major events by using the threshold seismicity rate such as N events per hour.

Data and methods

It has been found that regional catalogs of earthquakes obey the Gutenberg–Richter law (Gutenberg and Richter 1944; Wesnousky 1994). The Gutenberg–Richter law depicts that seismicity magnitudes distribute as an exponential relation with the number of seismicity (Gutenberg and Richter 1944). The magnitude frequency distribution, described by the Gutenberg–Richter law, is an empirical analysis method. It is a fundamental law in seismic hazard analysis and can indicate a relatively sensory process associated with seismic events of all magnitudes (Wesnousky 1994). The Omori law was initially proposed by Omori (1894). It is empirically determined as well and states that the rate of aftershocks decays as a power law with lapsed time (Shaw 1993). The modified form of the original Omori law is called the MOL, which incorporates other variables so that it can better applied to aftershock sequences (Utsu and Ogata 1995). The MOL can reliably describe the temporal variation of aftershock activities in terms of time-predictable patterns (Parsons 2002). The MOL model is able to assist in clarifying the correlation between stress transfer and seismicity rates (Kagan 2011). It has been widely used in seismic hazard assessment and seismicity forecast in recent years. Additionally, modifications based on the Omori law were proposed to analyze induced seismicity (Ouillon and Sornette 2005; Elisabeth 2011). The study assesses the uncertainties of the parameters in MOL and their posterior dependencies with respect to the observed aftershock sequences, and identified the trade-off between the c and p-value estimates (Holschneider et al. 2012). The MOL parameters depend on MOL time-dependent background rate, anisotropic aftershock triggering, temporally varying parameters, and finite duration of aftershock triggering. MOL parameters should be estimates for mining-induced seismicity to better serve the seismic hazard mitigation efforts in mines. We investigate the MOL parameters using seismicity sequences from the mining industry and evaluate the potential of using the MOL model as a tool for mining safety in terms of mining-induced seismicity. Additionally, due to the fact that the magnitude of completeness M_c (the cutoff magnitude) significantly affects the estimate of parameters, we introduce here how to apply a rigorous method for determining the optimal magnitude of completeness M_c (the cutoff magnitude) for a mining-induced seismicity sequence.

Site description

This study investigates mining-induced seismicity sequences of Creighton Mine, a deep nickel mine that is located near Sudbury, Ontario in Canada. We analyze the seismicity using the Gutenberg–Richter law with estimating the optimal completeness of magnitude and the MOL model. Details of the geological environment and structures of Creighton Mine have been described in previous studies (Malek et al. 2008; Ma et al. 2016). Considerable subsurface seismic occurrences with mining activity have been triggered by dynamic stress change along geological structures at Creighton Mine. A seismic monitoring network is located in Creighton Mine and it effectively monitors and records seismicity with high accuracy, providing a good basis for post analysis using geophysical tools.

Seismic monitoring system

The seismic monitoring networks at Creighton Mine are developed by ESG solutions and include a microseismic monitoring system and a ground motion system. The microseismic monitoring system is responsible for recording seismic events with small moment magnitudes from − 3 to + 1. The microseismic monitoring system consists of triaxial sensors and uniaxial sensors for the best balance of function and cost. The triaxial sensors are capable of measuring three directions and can monitor seismicity with recording waveforms that contain the information of source parameters, including magnitude, energy, source radius, and apparent stresses. The high accuracy and robust functions come at a price that triaxial sensors are more expensive than uniaxial sensors. In contrast, uniaxial sensors are installed in greater density for better localization and the magnitude estimation of seismic events. The microseismic monitoring system at the time of this study consists of 10 triaxial sensors and 52 uniaxial sensors to optimize the cost and performance of this system. The triaxial sensors are able to monitor a frequency range of 3–8000 Hz with sensitivity of 0.3 and 0.5 V/g. The uniaxial sensors can record in the frequency range of 500–5000 Hz with a sensitivity of 30 V/g. All sensors in this system together form a 104-channel mine-wide underground array. The depth distribution of sensors of the microseismic monitoring system roughly ranges from 1500 to 2400 m to guarantee a full coverage on the rock masses adjacent to main production elevations. Additionally, the ground motion system (Paladin system) is equipped to capture major events (high-magnitude seismic events) that are beyond the monitoring range of the microseismic monitoring system. In the ground motion system, three triaxial 4.5 Hz geophones are placed on the ground surface above the mine with a 24-bit data acquisition and recording system.

The association of these two systems ensures a coverage on a full magnitude range of all possible seismic events. The spatial distribution of sensors of the microseismic monitoring system is shown in Fig. 1. All microseismic data used in this study is from the events recorded by this seismic network.

Major events and aftershock sequence analysis

In our study, we investigate aftershock decay following major events and estimate the modified Omori model with determining the optimal magnitude of completeness M_c and the parameters change of the MOL model depending on M_c.

As a result of mining operations and geological structures such as joints and faults, Creighton Mine experienced very active seismicity during 2011. The seismicity catalog contains all seismic events in the whole mine. Two major events, which were both fault-slip type, were captured on July 6 and July 10, 2011. According to the cumulative and daily seismicity count, it is shown that seismicity accumulated around these two days and there was fast decay after the major events (Fig. 2). It is generally known that the aftershock volume depends on the magnitude of major events. According to comparing the magnitude and the aftershock volume of the two major events of Creighton Mine, we found that the magnitude and the aftershock volume is positively correlated (Fig. 2). The temporal distribution of seismicity at Creighton Mine within a long period of time for 7 months is shown in Fig. 2a. For better illustrating the major events and microseismicity, a short period of time for 60 days is plotted in Fig. 2b. The background seismicity rate of this seismicity sequence in Creighton Mine is 20 events per hour. We used this background seismicity rate as a criteria to define the end of the aftershock series. The number of aftershocks of Major Event 1 is 3048 and the moment magnitude ranges from − 2.15 to 0.8. For Major Event 2, the number of aftershocks is 2126 and the moment magnitude ranges from − 2 to 0.75.

For naturally occurring crustal earthquakes, the sequences usually stabilize in a certain duration of time and seismicity rates can abruptly increase around major earthquakes (Helmstetter and Sornette 2002). This accelerated seismicity is an important signature for forecasting large earthquakes. Similarly, sudden accumulation of induced seismicity can reflect the potential of the major-events occurrence in mines.

The frequency-magnitude distribution of seismicity is summarized by the Gutenberg–Richter law (Klein et al. 2006). The temporal distribution of magnitude and cumulative seismic moment of seismic events was analyzed and is plotted in Fig. 3. It is shown that the two days with major events experienced the largest cumulative seismic moment increase. Note that in order to avoid the influence on quantifying the cumulative seismic moment from the large magnitude of major events, the cumulative seismic moment calculation only included the microseismic events and ruled out the seismic moment of the two major events. The temporal, spatial, and magnitude information of the major events is listed in Table 1. According to the temporal distribution of Major Event 1 and Major Event 2, two seismicity sequences were compiled. The spatial distribution of post-event sequences of the major events is shown in Fig. 1. The aftershock sequence and its corresponding major event is plotted with a similar color. Since the magnitude of Major Event 1 is higher than Major Event 2, the microseismicity count of aftershock sequence of Major Event 1 is larger than that of Major Event 2. Before fitting the MOL model to the mining-induced seismicity of Creighton Mine, we first estimate the completeness of magnitude *M*c for each aftershock sequence based on Gutenberg–Richter law and the method developed by Wiemer (1997) to find the optimal *M*c. Then we apply the completeness of magnitude of each aftershock sequence to model the aftershock decay.

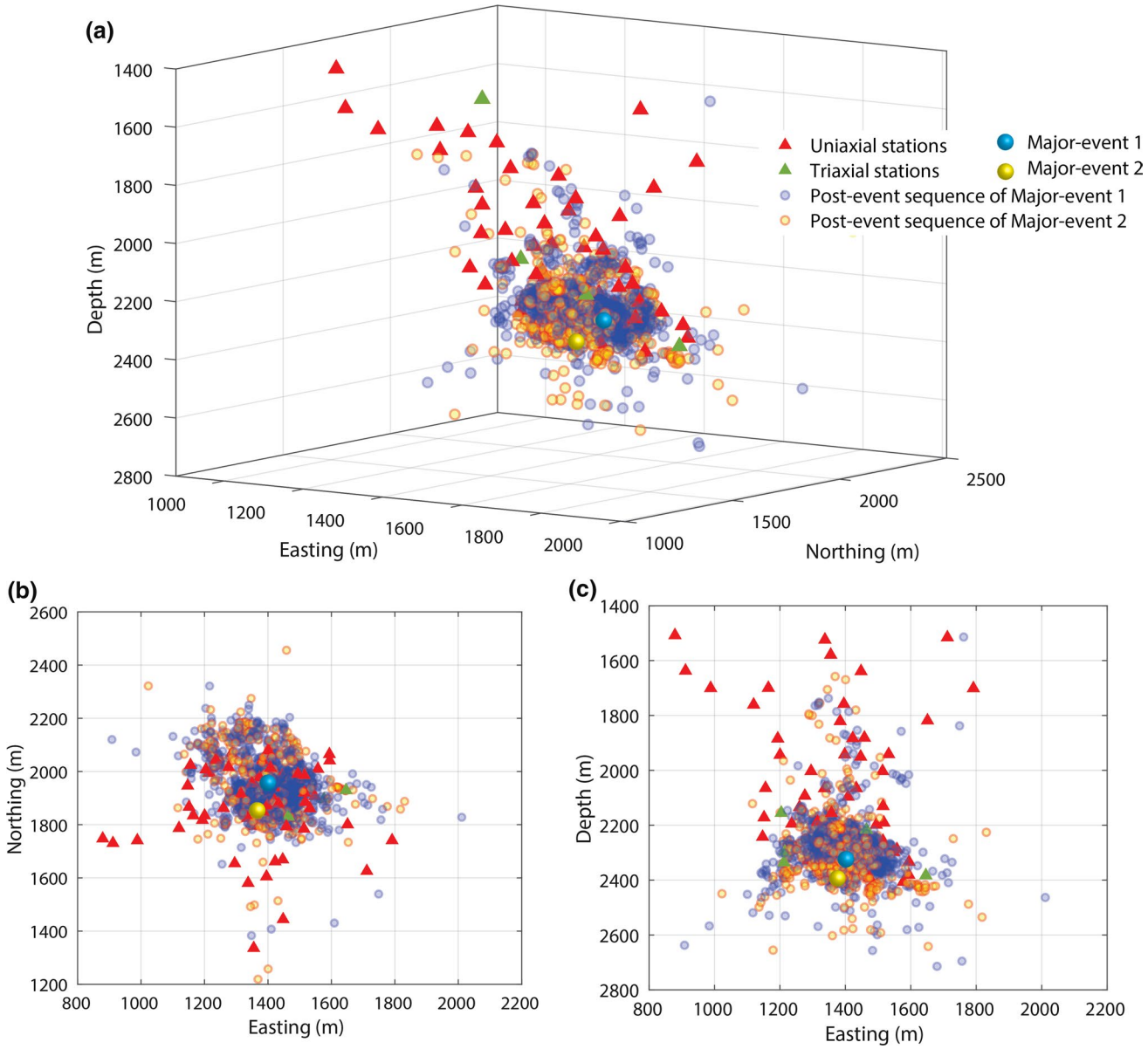

Fig. 1 **a** The 3D view, **b** the top view, and **c** the lateral view of the distribution of the seismic monitoring system, Major Event 1, Major Event 2, and their aftershock sequences at Creighton Mine

An important empirical observation on seismic events is the Gutenberg–Richter law, which interprets the proportional relationship between the magnitude M and the cumulative number of seismic events with magnitude larger than M:

$$\log N = a - bM, \tag{1}$$

where N is the cumulative number of events with magnitude equal to or greater than M; M is the completeness of magnitude; a and b are empirical constants. The b-value is the slope of linear fitting of frequency-magnitude relationship. For natural earthquakes, it is proved that b-value of the frequency-magnitude relationship of earthquakes is inversely proportional to stress (Wiemer and Wyss 1997). Previous studies found that b-values are in the range of $0.8 < b < 1.2$ and vary around 1.0 because of the heterogeneity and different stress conditions (Wiemer and Wyss 1997; Wesnousky 1999; Shcherbakov et al. 2004). The **a** values are the intercept of linear regression of frequency-magnitude and there is no physical mechanisms for a values. The temporal decay of aftershock activity is well defined by the MOL (Utsu and Seki 1954). The applicability of the MOL in mining-induced seismicity has been proven (Vallejos and McKinnon 2010, 2011).

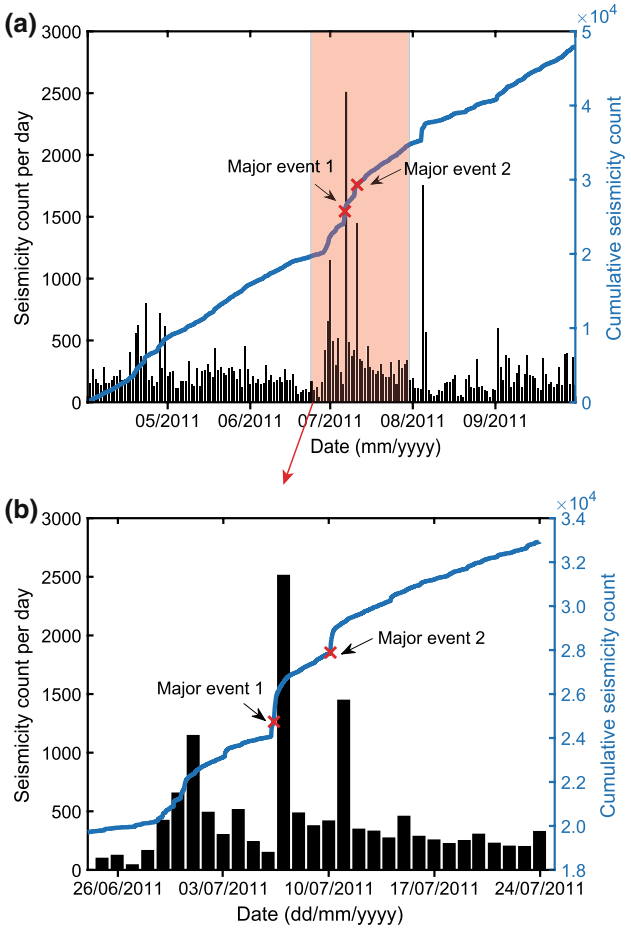

Fig. 2 Cumulative number of seismicity denoted by the line plot and seismicity rate per day denoted by the bar plot during **a** the extensive period of time (7 months) and **b** the target period of time (highlighted part in **a**) including two major events. The moment magnitude of Major Event 1 was 3.1 and Major Event 2 was with a smaller moment magnitude 1.4. Information about these two events is shown in Table 1

The MOL law was developed based on the Omori–Utsu aftershock decay formula in order to estimate the aftershock rate as a function of time in the temporal model (Utsu and Ogata 1995). In addition, it can be expanded as a function of combining time and space to be used in the spatial–temporal model. The Omori–Utsu formula describes the rate of aftershocks as:

$$\gamma = n(t) \equiv \frac{\mathrm{d}N}{\mathrm{d}t} = \frac{K}{(c+t)^p}, \tag{2}$$

where N is the cumulative number of seismic events in a specified region and time window, $r \equiv \mathrm{d}N/\mathrm{d}t$ is the rate of occurrence of aftershock, t is the time elapsed since the event, and p is the rate of decay. K and c are empirical parameters. The meaning of these parameters is interpreted in following parts. The MOL manifests the temporal correlations in aftershock sequences, which suggest the relaxation processes after the mainshock. The model was developed as a natural generalization of the Omori–Utsu formula, based on the hypothesis that any seismicity contributes to its own aftershocks; the number of aftershocks is attributed to the magnitude of the parent earthquake (Båth 1965).

The selection of magnitude of completeness M_c (cutoff magnitude) is crucial for the regression analysis using Gutenberg–Richter relationship and the aftershock decay. Several studies pointed out that an overestimate of M_c as a larger threshold results in the change of aftershock decay models (Zhuang et al. 2019; Wang and Manga 2010; Schoenberg 2013). An underestimate of the magnitude of completeness M_c, on the other hand, leads to incomplete aftershock sequences. This underestimate eventually biases the estimates of the productivity parameters because of the forfeit of a part of seismicity. Accordingly, choosing the optimal magnitude of completeness M_c rather than an overestimate or underestimate of the magnitude of completeness is a key initial step for following parameter estimate in mining-induced seismicity sequences.

Therefore, in this study, the magnitude of completeness M_c (cutoff magnitude) of the aftershock sequence is rigorously estimated using the maximum likelihood method (Shi and Bolt 1982, Ma 2016). We first calculate the b- and a-values of the G–R relationship with $M \geq M_i$. M_i means the picked magnitude for the corresponding b- and a-values. A magnitude bin of 0.1 is used to thoroughly examine all possible magnitude of completeness from − 2.5 to 0.8. A synthetic distribution is formed across a series of magnitude value and then the absolute difference between the observed and synthetic distribution in each magnitude bin is calculated to examine the goodness of fit. The detailed methodology of choosing the optimal magnitude of completeness is interpreted in a previous study (Ma 2016):

$$R(a,b,M_i) = 100 - \left(\frac{\sum_{M_i}^{M_{\max}} |B_i - S_i|}{\sum_i B_i} \times 100 \right), \tag{3}$$

where B_i is the observed cumulative number of events and S_i is the synthetic number of events in each magnitude bin. After determining the optimal magnitude of completeness, the aftershock decay modeling using the MOL is performed.

Since the values of parameters in the MOL analysis correspond to different seismicity sequences, the values of parameters k, p, and c are empirically determined (Utsu and Ogata 1995). It is assumed that a non-stationary Poisson process that N aftershocks occur at time t_i ($i = 1, 2, \ldots, N$) from the start time T_s and the end time T_e with intensity $m(t) = n(t)$, as shown in Eq. 4. The likelihood function is given as follows:

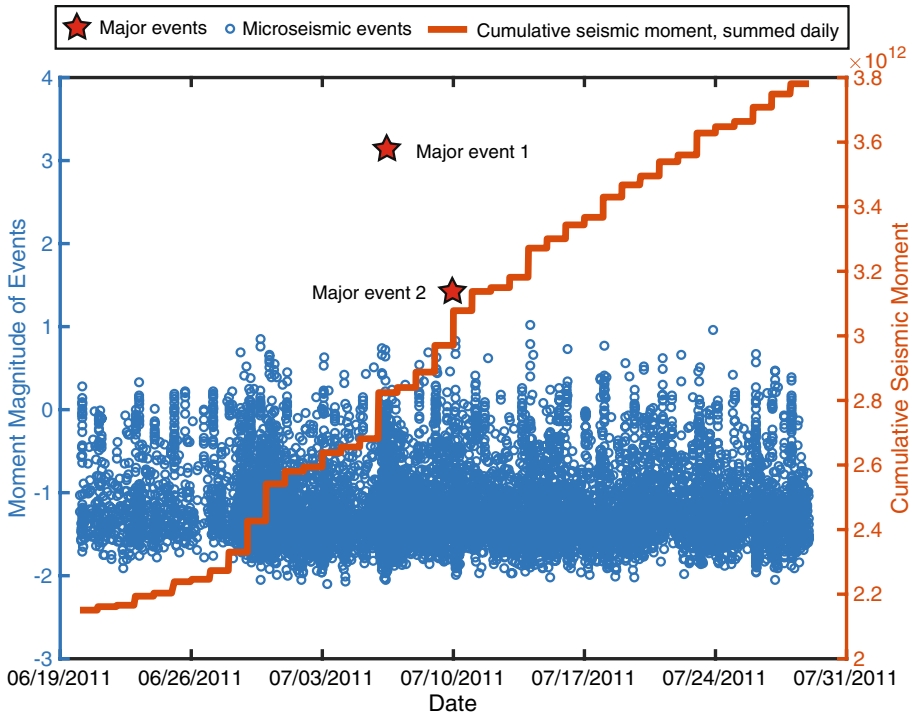

Fig. 3 Temporal daily distribution of moment magnitude of microseismic events associated with two major events, and temporal distribution of the cumulative seismic moment of all microseismic events

Table 1 Times, locations, and moment magnitude of major events at Creighton Mine

HMSE	Date	Time	North (m)	East (m)	Depth (m)	Moment magnitude
1	July 6, 2011	8:41 AM	1927	1399	2332	3.1
2	July 10, 2011	2:44 AM	1861	1384	2391	1.4

$$L = \left\{ \prod_{i=1}^{N} m(t_i) \right\} \exp - \left\{ - \int_{T_s}^{T_e} m(t) \mathrm{d}t \right\}. \tag{4}$$

We used the maximum likelihood method to estimate the values of k, p, and c. By maximizing the likelihood function lnL, it is requested that $\partial lnL/\partial K = 0$, $\partial lnL/\partial p = 0$, and $\partial lnL/\partial c = 0$, then Eqs. 5, 6, and 7 can be obtained. We determined the values of p, c and k by solving Eqs. 5, 6, and 7, which were originally from Eq. 2:

$$\sum_{i=1}^{N} \ln(t_i + c) - \frac{N}{p-1} - N \frac{\ln(T_s + c)(T_s + c)^{-p+1} - \ln(T_e + c)(T_e + c)^{-p+1}}{(T_s + c)^{-p+1} - (T_e + c)^{-p+1}} = 0, \tag{5}$$

$$p \sum_{i=1}^{N} \frac{1}{t_i + c} - \frac{N(p-1)\left\{(T_s + c)^{-p} - (T_e + c)^{-p}\right\}}{(T_s + c)^{-p+1} - (T_e + c)^{-p+1}} = 0, \tag{6}$$

$$k = \frac{N(p-1)}{(T_s + c)^{-p+1} - (T_e + c)^{-p+1}}. \tag{7}$$

Among them the exponent p is the most important parameter. The dependence of p was investigated and it was found that the exponent p increases as a function of the magnitude of major events. The physical interpretation of p is explained in that there is a faster decay rate following a major event than with a smaller magnitude.

Results and discussion

Magnitude distribution of two aftershock sequences

By estimating the goodness of fit for the magnitude distribution of two aftershock sequences using the maximum likelihood method, we obtain the optimal magnitude of completeness of − 1.5 for aftershock sequence of Major Event 1 and of − 1.6 for aftershock sequence of Major Event 2. Figure 4 exhibits how the goodness of fit changes along with the moment magnitude for aftershock sequence of Major Event 1 and Major Event 2, respectively. We apply the optimal magnitude of completeness as a threshold to determine the effective seismicity and perform

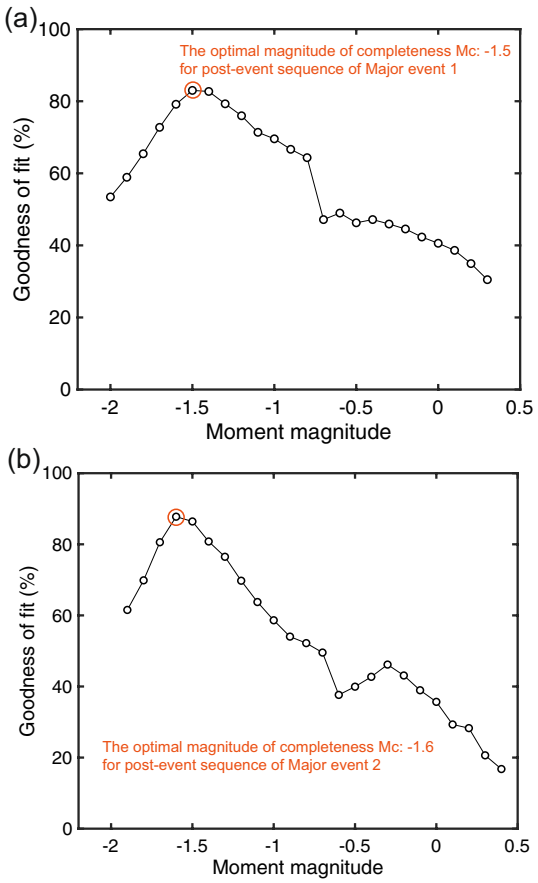

Fig. 4 The evaluation method for picking the optimal magnitude of completeness for aftershock sequence of **a** Major Event 1 and **b** Major Event 2 based on the goodness of fit using the maximum likelihood method

the linear regression using G-R law (Fig. 5). As shown in Fig. 5b, only the microseismicity with a magnitude higher than − 1.5 are allowed to for the use in the linear regression of G–R law for the aftershock sequence of Major Event 1. Similarly, the magnitude of completeness of − 1.6 is applied for the aftershock sequence of Major Event 2 (Fig. 5d).

Additionally, we visualize and illustrate the seismicity distribution versus the moment magnitude (Fig. 5a, c) to ensure that the significant part of the microseismicity is eligible with the cutoff magnitude (magnitude of completeness). The visualization of magnitude distribution validates that the analysis can take advantage of as much as possible information from the seismicity data in addition to meeting the criteria of the magnitude of completeness.

By performing the linear regression based on the number of seismic events and the magnitude, we compute and find that the *b*-value for aftershock sequence of Major Event 1 is 1.31 and the *b*-value for aftershock sequence of Major Event 2 is 1.50. It is generally known that the average *b*-value is about 1.0. High *b* values are generally associated with earthquake swarm activities. We compare the observed seismicity count and the synthetic seismicity count using fitted *b*-value and *a*-value. As shown in Fig. 6, the observed seismicity number and the synthetic seismicity number agree well from the magnitude of completeness. Schorlemmer and Wiemer (2005) expected that seismic *b*-value is an indicator of stress and is positively proportional to the deviatoric stress of σ_1–σ_3. Therefore, it can be inferred that the deviatoric stress immediately after the major events can maintain at a high level within a short period time (approximate 3–4 days). In addition, their study found that high *b*-values are correlated with the fault-slip type events. Although it has been determined by the ground motion monitoring system that these two major events in this study are the fault-slip type, the characteristic of high *b*-values verified again from the other perspective that these major events are the fault-slip type.

Aftershock decay

The decay patterns of aftershock sequences are investigated by applying the MOL with the eligible cumulative number of seismic events in the aftershock sequences. We establish the decay model based on the MOL and compare the predicted decay with the observed decay (practical decay) processes. The study of the aftershock decay can assist in understanding rock mass behavior such as stress relaxation in the aftershock decay process. Figure 7a and 7b demonstrates the modeling fit results for the aftershock of Major Event 1 and Major Event 2 at Creighton Mine. Our work shows that, as the aftershocks decay over time, the accumulating rate of seismic events decreases.

We estimate the parameters *p*, *c*, and *K* in the MOL, the accuracy of which is ensured because there are thousands of aftershocks for each magnitude interval on the premise of selecting the optimal magnitude of completeness. The aftershock sequences show that aftershock decay has the highest rate in the first 0.5 days. The period used for the modeling fit is around three days after each major event. The modeled cumulative aftershock decay with time closely agrees with the distribution of the observed cumulative number of aftershocks, especially during the early stage of the decay process (i.e., within the first day). The discrepancy between the fitted model and the observed cumulative numbers primarily appears during the middle temporal section in the decay process (Fig. 7a, b). The fitted model and the real cumulative numbers eventually match near the end of the decay process, when the seismicity rate decreases to 20 events/hour.

The MOL manifests the temporal correlations in aftershock sequences, suggesting the relaxation process after major events (Shcherbakov et al. 2005). During the occurrence of major events, the stress and the strain are enhanced in some regions neighboring the geological structures where

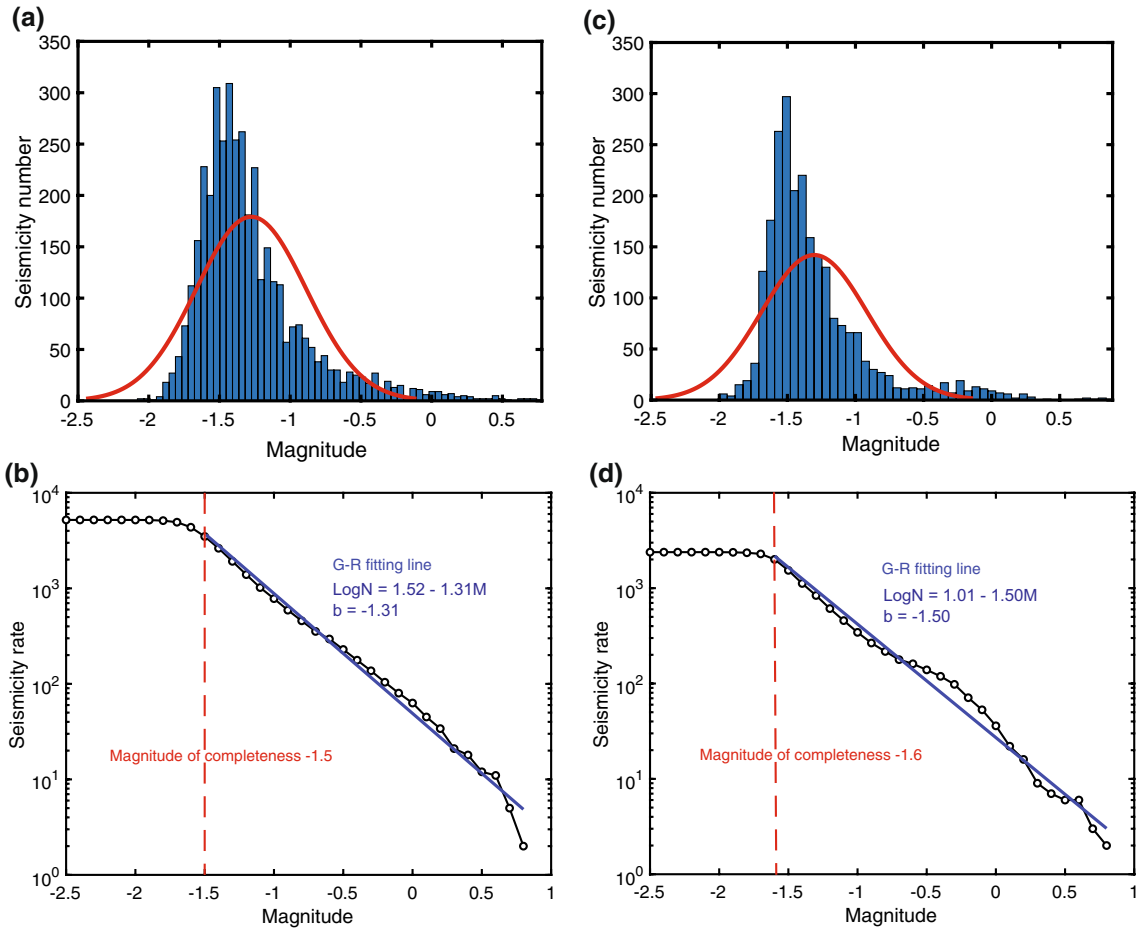

Fig. 5 Magnitude distribution of aftershock sequence of Major Event 1 and Major Event 2. **a** The number of seismicity versus magnitude for the aftershock sequence of Major Event 1; **b** Gutenberg–Richter recurrence relationship fitting for aftershock sequence of Major Event 1 and the magnitude of completeness of this aftershock sequence is − 1.5; **c** The number of seismicity versus magnitude for the aftershock sequence of Major Event 2; **d** Gutenberg–Richter recurrence relationship fitting for aftershock sequence of Major Event 2 and the magnitude of completeness of this aftershock sequence is − 1.6

major events are located. The stress relaxation is associated with the occurrence of aftershock. Aftershock activities assist to relieve the stress concentration arising from major events. All aftershock activities contribute to the reduction in the regional stress as a function of the magnitude of aftershock (Shcherbakov et al. 2005).

Utsu (1961) estimated p and c using 51 aftershock sequences and proposed that the p values ranged from 0.9 to 1.8. The most frequent values fell in the range from 1.1 to 1.4 (Utsu 1961). Previous studies demonstrated that the average p value ranges from 0.9 to 1.2 for major events with magnitudes ranging from 5 to 7.5 (Ouillon and Sornette 2005). By extending the MOL in mining-induced seismicity, it was measured that p is 0.4 for the aftershock sequence that occurred at Creighton Mine between October 1997 and March 1998 (Marsan et al. 1999). Hence it is inferred that during this time the aftershock decay in Creighton Mine was relatively slow. A $p > 1.0$ value indicates that the after-slip mechanism dominates the mainshock. A significantly smaller p value than 1.0 shows a slow decay and implies a viscoelastic relaxation mechanism following the mainshock (Morikami and Mitsui 2020). The aftershock decay pattern of the two major events in the 2011 timeframe is investigated to determine these related parameters. The predicted decay is compared with the observed decay to evaluate the applicability of the MOL to mining-induced seismicity at a deep hard-rock mine.

By investigating the aftershock sequences of Creighton Mine, the aftershock decay is found to agree well with the MOL. Parameters of the MOL for each major event were calculated and they are similar. The aftershock sequences of Major Event 1 take 3.8 days for the decay process. The aftershock sequences of Major Event 2 only needed 3 days to finish the decay process. A possible explanation is that Major Event 1 has a larger magnitude than Major Event 2, so Major Event 1 had a longer duration for the stress relaxation

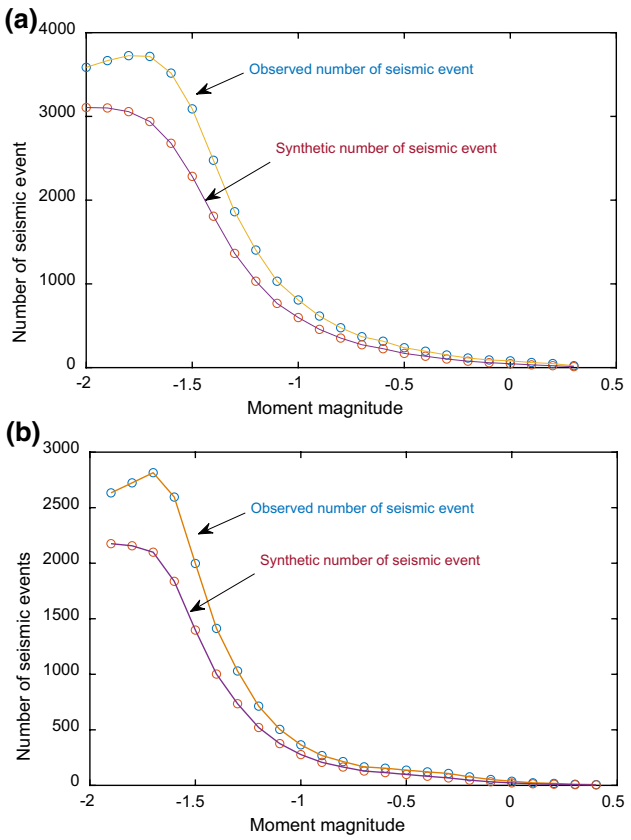

Fig. 6 The comparison of the observed seismicity count and the synthetic seismicity count using G-R fitting regression on aftershock sequence of **a** Major Event 1 and **b** Major Event 2

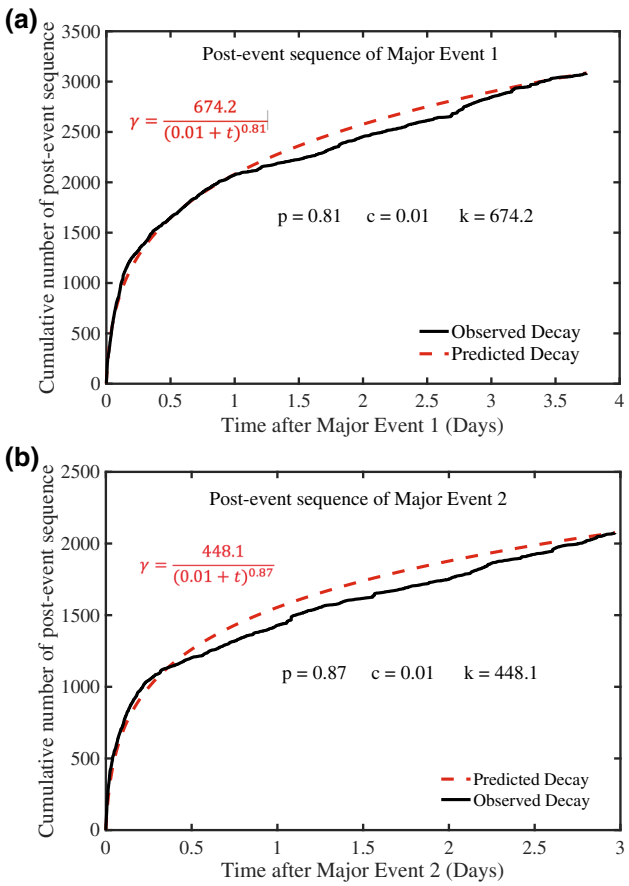

Fig. 7 Creighton Mine cumulative number of aftershock sequence decay with time modeling for **a** Major Event 1 and **b** Major Event 2. Lines in black: practical cumulative number of aftershock sequence; lines in red: fitted model using the MOL

process. This study discovers that aftershock decayed with an average $p = 0.84$ (p of Major Event 1 is 0.81; p of Major Event 2 is 0.87). According to the study of Vallejos and McKinnon (2009) for 18 seismically active mines in Canada, p controls the speed and p values range from 0.4 to 1.6 with average values between 0.74 and 1.05. The p values of Major Event 1 and 2 in Creighton Mine agree with their study well. A higher p value represents a faster decay rate and a shorter stress relaxation time. Good correlation is found between the p value and the aftershock decay. Major Event 1 with a p value of 0.81 exhibits a slower decay than Major Event 2 with a p value of 0.87 (Kisslinger and Jones 1991; Klein et al. 2006). In Marsan's study for Creighton Mine, a value of $p = 0.4$ was suggested and this relatively low value of p reflected a weak clustering on average (Marsan et al. 1999). As Marsan pointed out, p is computed as nearly 1 in most cases including crustal and induced earthquakes. This study indicates that the major events with a p value of ~ 0.8 have higher rates of decay than that in Marsan's previous study. The p values in this study are in the normal range of 0.7–1.1, as evaluated during a previous study (Klein et al. 2006). Two factors are likely to contribute to this change. One factor is that microseismicity in this study might form in shapes of stronger spatial clusters. The other factor of the change in p values is the changing conditions of mining operations, including the substantially greater excavation depths and different geological conditions. For instance, the current mining depth at Creighton Mine is several thousand meters deeper than when Marsan's study was performed. A previous study claimed that no direct evidence proves that p varies strongly with depth (Kisslinger and Jones 1991), whereas other work has pointed out that the sequences with deep major events have slightly larger p values than those at intermediate depths (Nyffenegger and Frohlich 2000). A comparison of this study with Marsan's work supports that depth dependence exists in seismic sequences at Creighton Mine. The K value of Major Event 1 and Major Event 2 is 647 and 448, respectively, during one day duration, which agree well with the summary of study in Vallejos and McKinnon (2009). The K values are found to range from 0 to 60 during one hour duration, which corresponds to 0–1440 during

one day duration. The *K* values of Major Event 1 and Major Event 2 fall in the range.

In this study of estimating the magnitude of completeness, we use the magnitude bin of 0.1 and this is the reason why the accuracy of the optimal magnitude of completeness is 0.1. For the aftershock sequence of current data sets, we suppose that a magnitude bin of 0.1 can meet the current need for Creighton Mine. A smaller magnitude bin for higher accuracy can be adjusted and employed accordingly depending on the number of seismicity sequence and the requirement of mine sites. Please note that applying a smaller magnitude bin generally demands more computational resources. Additionally, it should be noted that the MOL significantly rely on the historical seismicity sequences to establish the aftershock decay models. The parameters of the MOL for different mine sites are case by case. When expanding the study to another new mine site, the models still need to be optimized and calibrated with new parameters based on the maximum likelihood function.

Conclusions

This study investigates the aftershock decay of mining-induced seismicity after the occurrence of two major events at Creighton Mine. The results allow the following conclusions to be drawn:

- The magnitude of major events is a principal factor determining the cumulative seismic moment, cumulative number, and the decay pattern of aftershock sequence of mining induced seismicity. A major event is associated with a significant increase of seismic moment and seismic events number in its aftershock sequence. The magnitude of a major event is positively correlated with the cumulative seismic moment and the cumulative number of events. That is, a higher magnitude generally leads to a larger cumulative seismic magnitude and a larger density of seismic events.
- Before applying the MOL, the completeness of magnitude can be rigorously determined by evaluating the goodness of fit across different magnitudes using the maximum likelihood method. For different major events from a mine, although the magnitude of the major events is different, the completeness of magnitude is nearly the same for the aftershock sequence of different major events.
- The study of only two events can be considered only as a methodological work. In order to establish a reentry protocol in a future work, a statistical work for many events with different magnitudes and locations to establish the range of the MOL parameters is still need.

Acknowledgements The author Xu Ma acknowledge the China National Key Research and Development Program (Grant: 2021YFC3000603). Vale Canada Limited provided the field data for this study. Support for this project came from the Canadian Mining Industry Research Organization and a NIOSH Ground Control Capacity Building Grant (Contract 200-2011-40313). We thank Editor Savka Dineva for the insightful comments.

Declarations

Conflict of interest The authors declare that they have no conflict of interest.

References

Barton N, Pandey SK (2011) Numerical modelling of two stoping methods in two Indian mines using degradation of c and mobilization of φ based on Q-parameters. Int J Rock Mech Min Sci 48:1095–1112. https://doi.org/10.1016/J.IJRMMS.2011.07.002

Båth M (1965) Lateral inhomogeneities of the upper mantle. Tectonophysics 2(6):483–514

Beck DA, Brady BHG (2002) Evaluation and application and controlling parameters for seismic events in hard-rock mines. Int J Rock Mech Min Sci 39:633–642. https://doi.org/10.1016/S1365-1609(02)00061-8

Bogucki R, Lasek J, Milczek Jk, Tadeusiak M (2016). Early warning system for seismic events in coal mines using machine learning. In 2016 federated conference on computer science and information systems (FedCSIS) 2016 Sep 11 (pp. 213–220). IEEE

Brady BHG, Brown ET (2007) Rock mechanics and mining engineering. Rock mechanics for underground mining. Springer, Dordrecht, pp 1–16

Brady B, Leighton F (1977) Seismicity anomaly prior to a moderate rock burst: a case study. Int J Rock Mech Min Sci Geomech Abstr 14(3):127–132

Brown L, Hudyma M (2017a) Identifying local stress increase using a relative apparent stress ratio for populations of mining-induced seismic events. Can Geotech J 54:128–137. https://doi.org/10.1139/cgj-2016-0050

Brown L, Hudyma M (2017b) Identification of stress change within a rock mass through apparent stress of local seismic events. Rock Mech Rock Eng 50:81–88. https://doi.org/10.1007/s00603-016-1092-z

Disley N (2014). Seismic risk and hazard management at Kidd Mine. In: Proceedings of the seventh international conference on deep and high stress mining (107–121). Australian Centre for Geomechanics

Elisabeth C (2011) New approaches towards understanding and forecasting induced seismicity (Doctoral dissertation, ETH Zurich). https://doi.org/10.3929/ethz-a-006715437

Gutenberg B, Richter C (1944) Frequency of earthquakes in California. Bull Seismol Soc Am 34(4):185–188

Goebel THW, Schorlemmer D, Becker TW et al (2013) Acoustic emissions document stress changes over many seismic cycles in stick-slip experiments. Geophys Res Lett 40:2049–2054. https://doi.org/10.1002/grl.50507

Helmstetter A, Sornette D (2002) Subcritical and supercritical regimes in epidemic models of earthquake aftershocks. J Geophys Res Solid Earth 107(B10):ESE 10-1-ESE 10-21

Holschneider M, Narteau C, Shebalin P et al (2012) Bayesian analysis of the MOL. J Geophys Res Solid Earth. https://doi.org/10.1029/2011JB009054

Hudyma M, Potvin Y (2010) An engineering approach to seismic risk management in hardrock mines. Rock Mech Rock Eng 43(6):891–906

Kagan YY (2011) Random stress and Omori′ s law. Geophys J Int 186(3):1347–1364

Kisslinger C, Jones LM (1991) Properties of aftershock sequences in southern California. J Geophys Res Solid Earth 96(B7):11947–11958. https://doi.org/10.1029/91jb01200

Klein FW, Wright T, Nakata J (2006) Aftershock decay, productivity, and stress rates in Hawaii: indicators of temperature and stress from magma sources. J Geophys Res Solid Earth 111:1–26. https://doi.org/10.1029/2005JB003949

Llenos AL, Michael AJ (2013) Modeling earthquake rate changes in Oklahoma and Arkansas: possible signatures of induced seismicity. Bull Seismol Soc Am 103(5):2850–2861. https://doi.org/10.1785/0120130017

Luxbacher K, Westman E, Swanson P, Karfakis M (2008) Three-dimensional time-lapse velocity tomography of an underground longwall panel. Int J Rock Mech Min Sci 45:478–485. https://doi.org/10.1016/j.ijrmms.2007.07.015

Ma X, Westman EC, Fahrman BP, Thibodeau D (2016) Imaging of temporal stress redistribution due to triggered seismicity at a deep nickel mine. Geomech Energy Environ 5:55–64. https://doi.org/10.1016/j.gete.2016.01.001

Malek F, Espley S, Yao M, Trifu C (2008) Management of high stress and seismicity at Vale Inco Creighton Mine. In: The 42nd US rock mechanics symposium (USRMS). American rock mechanics association

Marsan D, Bean C, Steacy S (1999) Spatio-temporal analysis of stress diffusion in a mining-induced seismicity system. Geophys Res Lett 26(24):3697–3700

Morikami S, Mitsui Y (2020) Omori-like slow decay ($p < 1$) of post-seismic displacement rates following the 2011 Tohoku megathrust earthquake. Earth Planets Space 72(1):1–10. https://doi.org/10.1186/s40623-020-01162-w

Nyffenegger P, Frohlich C (2000) Aftershock occurrence rate decay properties for intermediate and deep earthquake sequences. Geophys Res Lett 27:1215–1218. https://doi.org/10.1029/1998GL010371

Omi T, Ogata Y, Hirata Y, Aihara K (2013) Forecasting large aftershocks within one day after the main shock. Sci Rep 3:2218. https://doi.org/10.1038/srep02218

Omori F (1894) On the after-shocks of earthquakes. J Coll Sci Imp Univ Jpn 7:111–200

Ouillon G, Sornette D (2005) Magnitude-dependent Omori law: theory and empirical study—magnitude-dependent Omori law. J Geophys Res Solid Earth. https://doi.org/10.1029/2004JB003311

Parsons T (2002) Global Omori law decay of triggered earthquakes: large aftershocks outside the classical aftershock zone: global Omori law decay of triggered earthquakes. J Geophys Res Solid Earth 107(B9):ESE 9-1-ESE 9-20. https://doi.org/10.1029/2001JB000646

Schoenberg FP (2013) Facilitated estimation of ETAS. Bull Seismol Soc Am 103(1):601–605. https://doi.org/10.1785/0120120146

Schorlemmer D, Wiemer S, Wyss M (2005) Variations in earthquake-size distribution across different stress regimes. Nature 437(7058):539–542. https://doi.org/10.1038/nature04094

Shaw B (1993) Generalized Omori law for aftershocks and foreshocks from a simple dynamics. Geophys Res Lett 20(10):907–910

Shcherbakov R, Turcotte DL, Rundle JB (2005) Aftershock statistics. Pure Appl Geophys 162:1051–1076. https://doi.org/10.1007/s00024-004-2661-8

Shcherbakov R, Turcotte DL, Rundle JB (2004) A generalized Omori's law for earthquake aftershock decay: a generalized Omori's law. Geophys Res Lett 31(11):n/a-n/a. https://doi.org/10.1029/2004GL019808

Shi Y, Bolt BA (1982) The standard error of the magnitude-frequency b value. Bull of the Seismol Soc Am 72(5):1677–1687. https://doi.org/10.1785/BSSA0720051677

Tierney R, Morkel G (2017) The optimisation and comparison of re-entry assessment methodologies for use in seismically active mines. In: Proceedings of the eighth international conference on deep and high stress mining (183–196). Australian centre for geomechanics

Urbancic T, Trifu C, Young R (1993) Microseismicity derived fault-planes and their relationship to focal mechanism, stress inversion, and geologic data. Geophys Res Lett 20(22):2475–2478

Utsu T (1961) A statistical study on the occurrence of aftershocks. Geophys Mag 30:521–605

Utsu T, Ogata Y (1995) The centenary of the Omori formula for a decay law of aftershock activity. J Phys Earth 43(1):1–33

Utsu T, Seki A (1954) A relation between the area of aftershock region and the energy of main shock. J Seism Soc Jpn 7:233–240

Vallejos JA, McKinnon SM (2009). Re-entry protocols for seismically active mines using statistical analysis of aftershock sequences. In rock engineering in difficult conditions. In: Proceedings of the 20th Canadian rock mechanics symposium, Toronto, Canada, paper (Vol. 4028)

Vallejos J, Estay R (2018) Seismic parameters of mining-induced aftershock sequences for re-entry protocol development. Pure Appl Geophys 175(3):793–811

Vallejos J, McKinnon S (2010) Omori's law applied to mining-induced seismicity and re-entry protocol development. Pure Appl Geophys 167:91–106. https://doi.org/10.1007/s00024-009-0010-7

Vallejos J, McKinnon S (2011) Correlations between mining and seismicity for re-entry protocol development. Int J Rock Mech 48(4):616–625

Wang C-Y, Manga M (2010) Earthquakes influenced by water. Springer, Heidelberg, pp 125–139

Wesnousky S (1994) The Gutenberg–Richter or characteristic earthquake distribution, which is it? Bull Seismol Soc Am 84(6):1940–1959

Wesnousky S (1999) Crustal deformation processes and the stability of the Gutenberg–Richter relationship. Bull Seismol Soc Am 89(4):1131–1137

Wiemer S, Wyss M (1997) Mapping the frequency-magnitude distribution in asperities: an improved technique to calculate recurrence times? J Geophys Res Solid Earth 102(B7):15115–15128. https://doi.org/10.1029/97jb00726

Xu YH, Cai M (2017) Influence of loading system stiffness on post-peak stress-strain curve of stable rock failures. Rock Mech Rock Eng 50:2255–2275. https://doi.org/10.1007/s00603-017-1231-1

Young RP, Maxwell SC (1992) Seismic characterization of a highly stressed rock mass using tomographic imaging and induced seismicity. J Geophys Res Earth 97:12361–12373

Zhuang J, Murru M, Falcone G, Guo Y (2019) An extensive study of clustering features of seismicity in Italy from 2005 to 2016. Geophys J Int 216(1):302–318